Research Article

# Excessive volume of hydrogel injectates may compromise the efficacy for the treatment of acute myocardial infarction

Peter Wise[1], Neil H. Davies[1], Mazin S. Sirry[2,3], Jeroen Kortsmit[1,#], Laura Dubuis[1,2], Chen-Ket Chai[4], Frank PT Baaijens[4], Thomas Franz[2,5,6,*]

**Short title**: Excessive injectate volume may compromise myocardial infaction therapy

[1]Chris Barnard Division of Cardiothoracic Surgery, University of Cape Town, Observatory, South Africa

[2]Division of Biomedical Engineering, Department of Human Biology, University of Cape Town, Observatory, South Africa

[3]Department of Biomedical Engineering, University of Medical Sciences and Technology, Khartoum, Sudan

[4]Department of Biomedical Engineering, Eindhoven University of Technology, Eindhoven, The Netherlands

[5]Research Office, University of Cape Town, Mowbray, South Africa

[6]Center for High Performance Computing, Rosebank, South Africa

[#] Claude Leon Postdoctoral Fellow

*Send correspondence to:
Thomas Franz, PhD
Department of Human Biology
Faculty of Health Sciences
University of Cape Town
Private Bag X3, 7935 Observatory, South Africa
Tel: +27 21 650 1795
E-mail: thomas.franz@uct.ac.za

This article has been accepted for publication and undergone full peer review but has not been through the copyediting, typesetting, pagination and proofreading process which may lead to differences between this version and the Version of Record. Please cite this article as Int. J. Numer. Meth. Biomed. Engng., e02772. doi: 10.1002/cnm.2772

## SUMMARY

Biomaterial injectates are promising as a therapy for myocardial infarction to inhibit the adverse ventricular remodeling. The current study explored interrelated effects of injectate volume and infarct size on treatment efficacy. A finite element model of a rat heart was utilized to represent ischemic infarcts of 10%, 20% and 38% of left ventricular wall volume and polyethylene glycol hydrogel injectates of 25%, 50% and 75% of the infarct volume. Ejection fraction was 49.7% in the healthy left ventricle and 44.9%, 46.4%, 47.4% and 47.3% in the untreated 10% infarct and treated with 25%, 50% and 75% injectate, respectively. Maximum end-systolic infarct fibre stress was 41.6, 53.4, 44.7, 44.0 and 45.3 kPa in the healthy heart, the untreated 10% infarct and when treated with the three injectate volumes, respectively. Treating the 10% and 38% infarcts with the 25% injectate volume reduced the maximum end-systolic fibre stress by 16.3% and 34.7% and the associated strain by 30.2% and 9.8%, respectively. The results indicate the existence of a threshold for injectate volume above which efficacy does not further increase but may decrease. The efficacy of an injectate in reducing infarct stress and strain changes with infarct size.

**Keywords**: biomaterial; polyethylene glycol; finite element method; cardiac function; ventricular remodelling; indentation tests

# 1 INTRODUCTION

Cardiovascular diseases have been the leading cause of deaths worldwide over the past decade. In 2008, myocardial infarction (MI) was responsible for about one third of these cardiovascular deaths, making it the leading cause of heart failure deaths. It is expected that there will be a drastic increase in deaths resulting from MI and cardiovascular diseases in Africa due to increasing economic wealth as well as an increase in obesity, diabetes and hypertension [1]. After MI, remodeling of the heart takes place in both the infarcted and healthy tissue in an attempt to regain functionality within the heart. The remodeling process comprises ventricular dilation and hypertrophy as well as the development of scar tissue in the region of the infarct, which affects the left ventricle (LV) and performance of the heart [2]. This remodeling process attempts to maintain the stroke volume and other cardiac function, but causes an increase in myocardial stress, as a results of wall thinning, LV dilation and increase in infarct stiffness [3, 4]. Current treatment therapies used for MI include both pharmaceutical and surgical techniques. Pharmaceutical therapies aim to prevent and treat any complications that may arise as a result of the infarction healing process, as well as aims to restore the balance between the oxygen supply and demand, preventing further ischemia [5]. Many surgical techniques on the other hand focus on the return of the blood flow to the infarcted region of the heart, for example coronary bypass grafting. Although these therapies are relatively effective 30-40% of patients die from heart failure within 1 year after being diagnosed [6]. Therefore, a new treatment to inhibit post-infarct remodeling has been investigated which involves the injection of biomaterials into the infarcted myocardium [7-9].

Various materials as well as cells have been used as therapeutic injectate [10, 11]. Cell therapies aiming at the regeneration of the infarcted myocardium [12, 13] have shown benefits but the underlying mechanisms remain uncertain. Computational analysis,

particularly the finite element analysis, has been an effective tool in investigating the mechanical aspects of acellular biomaterial injectate therapy for MI through model predictions. Recent computational investigations have shown that these injectates reduce the stress in the infarct [14-17]. However, the effects of injectate volume and a possible relationship between injectate volume and infarct size on the efficacy of the treatment are not well understood.

The current study aimed as such providing further insights into this question. It was hypothesized that there is an optimal volume, or volume range, of biomaterial delivered in an infarct to maximize the therapeutic effects, and that this optimal volume depends on the infarct size.

# 2 METHODS

## 2.1 Generation of finite element model of healthy heart from cardiac MRI

Sets of 11 cardiac short-axis magnetic resonance images (MRI) of the end-systolic and end-diastolic time points of a healthy rat heart were used from the study by Saleh et al. [18]. All institutional and national guidelines for the care and use of laboratory animals were followed for that study and approved by the institutional review board of the University of Cape Town.

Automatic image segmentation was undertaken on the end-systolic MRI set using *Segment* [19] to define the contours of the left ventricle (LV) endocardium, right ventricle (RV) endocardium and epicardium for each slice. Each segmented contour contained 80 data points which were exported as x, y and z coordinates. The data were imported into *Continuity* 6.4 (National Biomedical Computation Resource, University of California, San Diego, CA, USA) and prolate-spheroidal surface meshes were fitted to the contour points using an automated least-squares method. Minor manual adjustments were made on the mesh

to obtain a closer fit to the contour points by adjusting the derivatives as well as nodal locations. A small hole was created at the apex of the LV to omit redundant nodes. A three-dimensional mesh was created from the surface meshes. The mesh density was four by four by five elements in transmural, longitudinal and circumferential direction, respectively, yielding 80 tri-cubic Hermite elements with 127 nodes. The myofibrefibre orientation was implemented with tri-cubic Hermite basis functions rotating transmurally from -52° on the epicardial surface to 53° on the endocardial surface [20]. The definition of fibre orientation was simplified to avoid computational errors related to discontinuity in fibre orientation between septal wall and RV free wall [21]. The fibre orientations for the endocardial and epicardial surfaces were set while no constraints were defined for the fibre orientation on the endocardial surfaces of the RV, ensuring continuity of fibre angles throughout. Fig. 1 (a, b) illustrates the geometry of the biventricular rat heart model.

Boundary conditions were applied to the coordinates of the basal nodes as well as the derivatives in the circumferential and transmural directions of these nodes to limit the extension of the epicardial base and to simulate the effect of the stiff valve annuli. The derivatives of the apical nodes were fixed in longitudinal and circumferential directions such that the unrealistic effect of the apical hole was suppressed [22].

## 2.2 Material models

### 2.2.1 Myocardium

During the diastolic phase of the cardiac cycle, the heart undergoes purely passive expansion, which was described by a Lagrangian strain energy function [23] representing the transversely isotropic and nearly incompressible characteristics of the myocardium:

$$W_{myo} = \frac{1}{2} C\left(e^{Q} - 1\right) + C_{\mathrm{compr}}\left(J \ln J - J + 1\right), \qquad (1)$$

where $C$ is the stress scaling coefficient, $C_{compr}$ is the bulk modulus of the myocardial tissue and $J$ is the volume ratio of the stretch tensor **U** [24]. The second right-hand term in Eq. (1) is a penalty function to describe the passive myocardium as nearly incompressible [25]. $Q$ is given by

$$Q = b_{ff}E_{ff}^2 + b_{xx}\left(E_{cc}^2 + E_{ss}^2 + E_{cs}^2 + E_{sc}^2\right) + b_{fx}\left(E_{fc}^2 + E_{cf}^2 + E_{fs}^2 + E_{sf}^2\right) \quad (2)$$

where $E_{ff}$ is the fibrefibre strain, $E_{cc}$ is the cross fibrefibre in-plane strain, $E_{ss}$ is radial strain transverse to the fibrefibre direction. The shear strains are $E_{cs}$ in the transverse plane, $E_{fc}$ in the fibrefibre–cross-fibrefibre plane and $E_{fs}$ in the fibrefibre–radial plane. The parameters $b_{ff}$, $b_{xx}$ and $b_{fx}$ are the fibre strain coefficient, cross-fibre strain coefficient and shear strain coefficient, respectively. Material properties used in this study were $C$ = 2.0 kPa, $b_{ff}$ =9.2, $b_{xx}$ = 3.0, $b_{fx}$ = 3.7 based on Omens et al. [20] with some modifications to match the model predicted stress and strain to the data reported Omens et al. [20]. $C_{compr}$ was set to 100 kPa. Active contraction during the systolic phase was described by an additional fibre directional active tension component given by

$$T_0 = \frac{1}{2}T_{max}\frac{Ca_0^2}{Ca_0^2 + ECa_{50}^2}\left\{1 - \cos\left[\left(\frac{t - t_0}{ml_r\sqrt{2E_{11} + 1} + b}\right)\pi\right]\right\}, \quad (3)$$

with

$$ECa_{50} = \frac{Ca_{0,max}}{\sqrt{\exp\left[B\left(l_r\sqrt{2E_{11} + 1} - l_0\right)\right] - 1}}. \quad (4)$$

Here, $m$ is the gradient and $b$ is the time-intercept of the linear relationship of relaxation duration to sarcomere length, with $m$ = 1.0489 s/μm and $b$ = -1.429 s [26]. $B$ = 4.75 $\mu m^{-1}$ describes the shape of the relationship of peak isometric tension to sarcomere length [26]. $Ca_{0,max}$ = 4.35 μmol/l is the maximum peak concentration of intracellular calcium [27]. $l_r$ =

1.85 μm [26] and $l_0$ = 1.58 μm [28] are the sarcomere length at its stress-free state and at zero tension, respectively. Additionally, $T_{max}$ = 135.7 kPa [26] and $Ca_0 = Ca_{0,max}$ = 4.35 μmol/l [27].

### 2.2.2 Polyethylene Glycol Hydrogel

***Material preparation and experimental characterization***

Vinyl sulfone derivatized polyethylene glycol (PEG) prepared by methods described by Dobner et al. [8] In brief, a 5% PEG (20 kPa, 8-arm, hydroxyl-terminated: 20PEG-8OH, Shearwater/Nektar) solution in dry dichloromethane was reacted with 5x molar excess of sodium hydride followed by 50x molar excess of divinyl sulfone under inert atmosphere for 48 hours. After neutralization of the remaining sodium hydride with glacial acetic acid and removal of the precipitated sodium acetate salt through centrifugation and vacuum filtration, reduction of the volume by rotary evaporation, and precipitation in 10x excess cold diethyl ether, the product was dried (room temperature, 24 hours, reduced pressure). Purification of the product (20PEG-8VS) was achieved through 3x re-precipitation from dichloromethane in diethyl ether and drying. Gels of 10% (m/v) nominal concentration were prepared by dissolving 10 mg of 20PEG-8VS in 50 μL phosphate-buffered saline, and casted into discs with diameter of 5 mm and thickness of 2 mm.

Using a customized set-up adopted from Cox et al. [29], the PEG hydrogel discs (n = 6) were subjected to quasi-static indentation tests at the center of the disc (spherical indenter, diameter: 2 mm; displacement rate: 0.01 mm/s). After preconditioning, three consecutive indentations with a maximum indentation depth of 0.5 mm were conducted for each sample. Additional indentation tests were performed at two off-center locations for each sample, providing the same results as the central indentation. The average reaction force of the central

indentations at the indentation depths of 0.1, 0.3 and 0.5 mm (data are provided as an online supplement) was used for the identification of constitutive parameters.

***Determination of constitutive parameters using an inverse finite element method***

The hydrogel was described by the isotropic Neo-Hookean hyperelastic strain energy function

$$W_{gel} = C_{10}(\overline{I}_1 - 3) + \frac{1}{D}(J-1)^2, \tag{5}$$

where $\overline{I}_1 = tr(\overline{F}\cdot\overline{F}^t)$ is the first deviatoric invariant, $J = \det(F)$ is the volume ratio, $F$ is the deformation gradient, $\overline{F} = J^{-\frac{1}{3}}F$ is the deviatoric deformation gradient, $C_{10}$ and $D$ are the Neo-Hookean elastic and compressible moduli, respectively.

An axisymmetric finite element model of the hydrogel disc sample and a rigid body indenter was used to simulate the indentation experiments (Abaqus 6.10, Dassault Systèmes, Providence, RI, USA). Hybrid elements were used to account for the nearly-incompressible behavior of the gel. Using the objective function

$$C_f = \sum_{i=1}^{3}\left(\frac{F_i^{\text{num}} - F_i^{\text{ex}}}{F_i^{\text{ex}}}\right)^2 \tag{6}$$

and setting $D$ = 0.8 MPa$^{-1}$, the constitutive parameters were identified through fitting of the numerical solution to the experimental force-displacement data averaged over all samples and tests. In Eq. (6), $F_i^{\text{num}}$ and $F_i^{\text{ex}}$ are the reaction forces from numerical simulation and experiment, respectively, at three indentation depths ($i$ = 1 to 3) of 20%, 60% and 100% of the sample thickness which corresponded to 0.1, 0.3 and 0.5 mm, respectively. Minimizing the cost function with a Nelder-Mead simplex algorithm resulted in $C_{10}$ = 0.0123 MPa.

### 2.2.3 Homogenization of myocardium and hydrogel injectate

When injected into early ischemic infarcts, hydrogel has been found to form very thin layers within the myocardial tissue [8, 9, 30]. Hence, the infarcted myocardium with dispersed hydrogel was represented using a homogenization approach based on the fractions and constitutive relationships of the different materials within the hydrogel-treated region of the LV.

For the distinction between healthy myocardium, infarcted myocardium and hydrogel, a strain energy function with three terms was formulated that could be used to describe any of the three materials and mixtures thereof:

$$W = \alpha \cdot W_{\text{healthy}} + \beta \cdot W_{\text{infarct}} + \gamma \cdot W_{gel} \ , \tag{7}$$

with $\alpha + \beta + \gamma = 1$. The parameters $\alpha$, $\beta$ and $\gamma$ represent the fractions of healthy myocardium, infarcted myocardium and hydrogel injectate, respectively. $W_{\text{healthy}}$ and $W_{\text{infarct}}$ describe the constitutive properties of healthy and infarcted myocardium according to section 2.2.1 and 2.3, and $W_{\text{gel}}$ represents the hydrogel according to Eq. (6).

## 2.3 Implementation of infarcts and hydrogel injectates

Three sizes of antero-apical transmural infarcts were implemented in the LV, namely 10%, 20% and 38% of the LV wall volume (Fig. 1 c-e). The infarct region and functional border zone were defined employing a matrix of 5 x 5 x 5 field variables [31] in each element allowing for intra-element material status changes. The size of the border zone was approximated to 10% of the infract size.

This study focused on early ischemic infarcts (e.g. few minutes to hours after MI onset), the mechanical properties of which are characterised by the loss in contractility and dominated

by the passive material properties of myocardium [2]. Therefore, the constitutive changes for the infarct were limited to the active tension relationship Eq. (3). Infarcts were assumed to be completely non-contractile. This was modelled by turning off the active contraction, i.e. setting the intracellular calcium concentration $Ca_0 = 0$. The functional border zone was assumed to have partial contractile dysfunction modelled by reducing the intracellular calcium concentration to 50% of the value of the healthy case.

The volume fractions of dispersed hydrogel and infarcted tissue within the hydrogel-treated region were obtained from morphometric analysis of histological micrographs from a previous study [32]. All institutional and national guidelines for the care and use of laboratory animals were followed for that study and approved by the institutional review board of the University of Cape Town. In brief, after experimental infarction by ligation of the left anterior descending artery, PEG hydrogel was immediately injected in the infarcted wall and allowed to disperse and polymerize *in situ* for 30 min. The heart was harvested and cryosectioned from the apex towards the base obtaining 30 μm sections the heart at 20 levels with an inter-level distance of 200 μm. Microscopic images of DAPI (4',6-diamidino-2-phenylindole) mounted sections were acquired with an Eclipse 90i Fluorescent Microscope with digital camera DXM-1200C and fluorescein isothiocyanate filter (Nikon Corporation, Tokyo, Japan) at x3.2 magnification and stitched to composite images of the entire short-axis cross section of the heart at each level. The composite images from three levels of the heart underwent morphometric assessment. For each image, a region of interest was defined in the infarct region (Simpleware, Simpleware Ltd, Exeter, UK) that contained a representative distribution of the hydrogel. Two-dimensional masks of tissue and hydrogel were defined in the region of interest and the respective areas were measured. The fractions of infarcted tissue and hydrogel were found to be $0.558 \pm 0.052$ and $0.442 \pm 0.042$ (mean ± standard deviation), respectively. These fractions were employed in the homogenization constitutive relationship,

Eq. (7), by setting $\beta = 0.558$ and $\gamma = 0.442$ to model the material properties of the hydrogel-treated infarct region.

A local wall thickening was implemented in the model geometry to account for the volume of the injected hydrogel. This was performed by applying a negative pressure to both the endocardial side and the epicardial side of the wall at the region of injection. All nodal points except those in the area of injection were constrained to ensure the thickening was applied locally to the region where injection occurred.

### 2.4 Study cases

To determine the effect of injectate volumes on infarct mechanics, three hydrogel injectate volumes were studied, namely 25%, 50% and 75% of the infarcted wall volume. These injectate volumes were implemented in the 10% infarct size, as illustrated in Fig. 1 (f-h). The injectate-treated regions were modelled centralized within the infarct region. Furthermore, to evaluate the effect of the variable infarct size, two additional cases were developed with larger infarcts: a) 25% injectate volume was implemented in the 38% infarct, and b) 50% injectate volume was implemented in the 20% infarct.

### 2.5 Left ventricular hemodynamics

A linear increase in pressure was applied to the left and right ventricles cavities to simulate the diastolic phase of the cardiac cycle. The LV and RV end-diastolic pressures were taken to be 3.36 and 1.78 kPa, respectively, which gave an end-diastolic volumes equal to those recorded from the MRI. To simulate the systole, active contraction was applied with constant LV and RV volume until a desired LV peak pressure of 14 kPa was reached. These pressure

end points were used for all models based on the understanding that the LV pressure needs to overcome the aortic pressure for the aortic valve to open.

The analysis of the cardiac hemodynamics was performed by recording the pressure–volume relationships marked by the diastolic and systolic phases of the LV cardiac cycle. The end-diastolic pressure volume relationship (EDPVR) provided a measure of the ventricular compliance whereas the contractility, or elastance, $E_{max}$ was defined by the slope of the end-systolic pressure volume relationship (ESPVR) curve. Other cardiac functional parameters obtained from EDPVR and ESPVR were the dead space volume $V_0$, stroke volume SV and ejection fraction EF.

# 3 RESULTS

## 3.1 Left ventricular hemodynamics

Fig. 2 (a) displays the pressure volume relationships of the healthy case and the three infarct sizes 10%, 20% and 38%. The EDPVR was identical for all cases since the ischemic infarcts exhibited the same passive material properties as the healthy tissue. For end-systolic, a slight decrease in the slope of the ESPVR curves was observed with increasing infarct size. Fig. **2** (b-e) shows the effect of infarct size on ejection fraction (EF), dead volume ($V_0$), stroke volume (SV) and end-systolic elastance ($E_{max}$). With increasing infarct size, similar steady decreases were recorded for EF and SV whereas $E_{max}$ decreases primarily for the 38% infarct and $V_0$ was shown to increase.

Fig. 2 (f, g) illustrates end-diastolic and end-systolic pressure volume relationships for the untreated and treated 10% infarct cases as well as the healthy control. The end-diastolic compliance was lower in the treated infarct cases compared to the untreated infarct and

decreased with an increase in injectate volume (Fig. 2 f). The systolic function of the infarcted LV was recovered, to varying extent, for the cases with hydrogel injectate.

The left ventricle functional parameters for different models are summarized in Table 1. For the treated 10% infarcts, $E_{max}$ increased steadily with increasing injectate volume exceeding the value of the healthy control for the 50% and 75% injectate. The dead volume and ejection fraction were improved for all injectate sizes; the greatest benefit was observed for the 50% injectate. Comparing between the 25% relative injectate volume in the 10% and 38% infarcts, the EF improvement was similar; 3.3% and .3.5% respectively. The EF recovery in absolute measures was, however, considerably smaller for the 38% infarct due to the larger associated functional loss (48.1%) as opposed to 9.7% loss in the 10% infarct when compared to the healthy case. A large difference in improvement of EF was observed for the 50% relative hydrogel volume in the 10% infarct (5.6%) and the 20% infarct (39%). In both 20% and 30% infarcts, the injectate also improved the stroke volume unlike the further decrease in stroke volume observed in the treated 10% infarct. A further difference was the decrease in the end-systolic elastance $E_{max}$ in the presence of the injectates for the 38% infarct and 20% infarct in contrast to the increase of $E_{max}$ in the 10% infarct with the respective injectate volume. The improvement of dead volume in different infarct sizes was similar for each of the two injectate volumes which, once again, did not correspond to a similar absolute recovery due to the increase in functional impairment with increasing infarct size.

[Position of **Table 1**]

### 3.2 Myocardial mechanics

End-diastolic strain was calculated with the end-systole as a reference configuration and vice versa for end-systolic strain. Fig. 3 illustrates the end-diastolic and end-systolic maximum

fibre stress and strain for the 10% infarct cases without injectate and with 25%, 50% and 75% injectate volumes, respectively, and the healthy control. At the end-diastolic time point, stress and strain were the same in the healthy case and the untreated infarct and decreased with increasing injectate volume. At end-systole, the stress in the untreated infarct exceeded the level predicted for healthy control. In the treated infarcts, the stress was reduced compared to the untreated infarct and were only slightly higher than in the healthy case. Although marginally, the largest decrease was observed with the 50% hydrogel injectate. The end-systolic strain was predicted to be lower in all treated infarcts compared to the untreated infarct. Similar to stress, the largest decrease in strain was observed for the 50% injectate whereas the least decrease found for the 75% injectate volume.

A comparison of the myocardial mechanics for different infarct sizes with the same relative injectate volume is provided in Fig. 4 and Fig. 5. The maximum fibre stress and strain in the 10% and 38% infarcts when treated with the 25% injectate are illustrated in Fig. 4. The injectate led to a decrease of the end-diastolic stress in the 10% infarct but not in the 38% infarct. The end-diastolic strain was reduced in both the 10% and 38% treated infarcts, by 20.3% and 25.7%, respectively, compared to the untreated infarct. The decrease in the end-systolic stress observed in the treated 38% infarct was 34.7% compared to the untreated case whereas a smaller decreases of 16.7% was predicted in the treated 10% infarct. However, the stress level in the treated 10% infarct dropped nearly to the healthy level whereas in the large treated infarct the stress still considerably higher than in the healthy control. The end-systolic strain was positive in all infarcts compared to negative strain in the healthy case. The end-systolic strain decreased by 30.2% from untreated to treated 10% infarct but only by 9.8% in the case of the 38% infarct.

The maximum fibre stress and strain in the 10% and 28% infarcts when treated with the 50% injectate are illustrated in Fig. 5. The end-diastolic stress and strain were predicted to be lower in both treated infarcts compared to the untreated infarcts and healthy controls. At end-systole, the reduction of stress from untreated to treated case was considerably higher in the 20% infarct (40.3%) compared to the 10% infarct (17.6%). The opposite was observed for end-systolic strain: a larger reduction for the 10% infarct (44.4%) than for the 20% infarct (18.6%).

## 4 DISCUSSION

The assessment and optimization of the therapeutic effects of biomaterial injections on the function and mechanics of an infarcted heart has been a subject of various computational studies [14, 15, 33, 34]. However, no study was found that evaluated the relationship of injectate volume and infarct size in the context of the therapeutic benefit. The current computational study investigated the effect that the variation in volume of biomaterial injectates has on improvement of ventricular performance and wall mechanics in an infarcted rat heart. We employed a particular formulation of PEG hydrogel used in our *in vivo* preclinical research [8]. The study utilized biventricular finite element models of a healthy heart and hearts with an ischemic infarct with the size of 10%, 20% and 38% of the LV myocardial volume, respectively. The 10% infarct size was studied as untreated (i.e. without injectate) and treated with a PEG hydrogel injectate the volume of which was 25%, 50% and 75% of the infarct wall volume. This design facilitated a controlled comparison of untreated infarcts, treated infarcts and a healthy control case. Additionally, the 25% and 50% hydrogel injectate volumes were implemented in 38% and 20% infarct sizes, respectively, and compared to the treated 10% infarct counterparts to study the effect of the relative injectate volume on variable infarct sizes. As the same passive constitutive properties were used for

the early infarct and the healthy tissue, passive diastolic mechanics was the same in infarct and healthy cases and the analysis of the injectate benefits focused particularly on end-systolic stage.

In contrast to our previous work [16, 17], we represented the hydrogel injectates in a homogenized mixture approach. We developed and implemented in *Continuity* a mixed-term constitutive framework (Eq. 7). The framework combined a transversely isotropic strain energy function and active tension for myocardium and a Neo-Hookean strain energy function for the isotropic hydrogel. The framework allowed to describe healthy contractile myocardium, infarcted myocardium, infarcted myocardium with biomaterial injectate and the functional border zone by using three parameters that determine ventricular region to be described. The ratio of injected material to infarcted tissue, i.e. 55.8% to 44.2%, was determined in histological sections of an ischemic infarct with immediately injected PEG hydrogel [32]. The parameter values of the Neo-Hookean material model used for the injectate were obtained from the experimental characterization of PEG hydrogel that was also used *in vivo* [8].

We found an increase of the beneficial effects of the hydrogel injectate, both for ventricular function and infarct wall mechanics, with increasing the injection volume from 25% to 50% of the infarct wall volume. However, the benefit did not increase further for an injectate volume of 75%. The ejection fraction of the 10% infarct increased by 3.3% with the 25% hydrogel injectate and by 5.6% with the 50% injectate whereas it slightly dropped to 5.3% for the 75% injectate. Also increasing the injectate volume from 50% to 75% did not further elevate the ESPVR curve (Fig. 2g) compared with the elevation observed between 25% and 50%. Similar trends were predicted for infarct strain and stress at end systole (Fig. 3 e and f) with the 50% injectate resulting in the largest benefit. The end-systolic maximum fibre strain

in the 10% infarct was reduced by 44.4% for the 50% injectate compared to 30.2% and 21.7% for the 25% and 75% injectate. For the maximum end-systolic fibre stress, differences were more moderate: 17.6%, 16.3% and 15.1% reduction for the 50%, 25% and 75% injectate. This indicates the existence of an optimal amount of biomaterial to be delivered above which the injectate's benefits may not further increase or may even decrease. This finding is supported by results of Wenk et al. [33] in a study utilizing a canine LV model. Investigating the optimal pattern of intra-myocardial injectates with total volume of 0.18 mL and 5.4 mL, the maximum benefit was reported for an injectate pattern with an intermediate number of inclusions when optimizing for myofibre stress and stroke volume. Lee et al. [34] predicted in a patient-specific computational model that the magnitude and the heterogeneity of the myofibre stress in the area of biomaterial inclusions decreases with decreasing injectate volume. This similarly indicates that an increasing injectate volume can have adverse effect on therapeutic efficacy.

Comparing the effects of the same injectate volume (normalized to the infarct volume) on end-systolic mechanics for different infarct sizes, we found that the attenuating effect of the injectate decreased with infarct size for the end-systolic fibre strain but increased with infarct size for the associated fibre stress. The 25% injectate reduced the end-systolic strain by 30.2% and 9.8% in the 10% and 38% infarct, respectively (Fig. 4 f). Similarly, the 50% injectate reduced the maximum fibre strain by 44.4% in the 10% infarct and by 18.6% in the 20% infarct (Fig. 5 f). However, the 25% injectate decreased the maximum fibre stress by 16.3% and 34.7% in the 10% and 38% infarct, respectively (Fig. 4 e). The 50% injectate reduced the maximum fibre stress by 17.6% and 40.3% in 10% and 20% infarct (Fig. 5 e). The opposite effects for attenuation of strain and stress with infarct size can be explained by the increase in fibre strain with infarct size in combination with the increase of myocardial stiffness with increasing strain based on the exponential stress-strain relationship (Eq. 1). A

smaller reduction in strain at higher strain levels in the larger infarcts compared to the small infarct can indeed result in a larger decrease in stress in the larger infarcts. The diminution of the strain reduction effect of the injectate with increasing infarct size may be based on the dissimilar absolute sizes of supported and unsupported infarct regions. These resulting difference in endocardial forces on and boundary conditions of the infarct lead to different deformation of the infarct in particular when considering that the infarct wall thickness remains independent of infarct size.

A major limitation of the current study is the lack of comprehensive characterization of the interaction between the infarct size and injection volume. In the current study we showed three injectate volumes with the 10% infarct with two selectively added cases (i.e. I20-G50 and I38-G25). Although the presented work allowed exploring the effect of excessive injectate volume with providing a clue of what the effect of varying the infarct size could be, they left unresolved questions with regards to the role the infarct size could play.

The positively outlying functional data of I20-G50 case is based on a large recovery of ESV (ca 21%) and a small recovery of EDV (ca 7%) when compared to the non-treated I20 infarct case. Although the reason for this is not fully understood and requires further investigations, it may be partially related to inconsistencies between different cases in the change of the LV geometry associated with the implementation of the added biomaterial volume. The different infarct sizes and injectate volumes lead to varying degrees of epi- and endocardial bulging, the latter of which translates into different degrees of reduction of the LV cavity volume.

## 5 CONCLUSIONS

The results of this study indicate that a threshold may exist for the volume of biomaterial injectates for treatment of acute myocardial infarction. For volumes exceeding that threshold, the therapeutic efficacy of the treatment does not further increase but may even decrease - both in terms of ventricular function and wall mechanics. In addition, the efficacy of biomaterial injectates in terms of reducing wall stress in the infarct was shown to increase with infarct size.


## ACKNOWLEDGEMENTS

The authors would like to thank Muhammad Saleh and Prof Ernesta Meintjes from the UCT/MRC Medical Imaging Research Unit, Department of Human Biology, University of Cape Town, for providing the cardiac MRI data of the rat heart. Dr Roy Kerckhoffs and Jeff Van Dorn from the Cardiac Mechanics Research Group, University of California in San Diego, are acknowledged for support and advice with cardiac modelling using *Continuity*. JK acknowledges a postdoctoral fellowship of the Claude Leon Foundation. This work was supported by a grant from the Center for High Performance Computing, Council for Scientific and Industrial Research, South Africa. NHD acknowledges the South African Medical Research Council.


## CONFLICT OF INTEREST

All authors declare that they do not have conflicts of interest.

## REFERENCES


1. Steyn K, Sliwa K, Hawken S, Commerford P, Onen C, Damasceno A, Ounpuu S, Yusuf S, for the INTERHEART Investigators in Africa. Risk factors associated with myocardial infarction in africa: The interheart africa study. *Circulation* 2005; **112**:3554-3561. DOI:10.1161/circulationaha.105.563452.

2. Holmes JW, Borg TK, Covell JW. Structure and mechanics of healing myocardial infarcts. *Annual Review of Biomedical Engineering* 2005; **7**:223-253.

3. Pfeffer MA, Braunwald E. Ventricular remodeling after myocardial infarction. Experimental observations and clinical implications. *Circulation* 1990; **81**:1161.

4. Opie LH, Commerford PJ, Gersh BJ, Pfeffer MA. Controversies in ventricular remodelling. *Lancet* 2006; **367**:356-367.

5. Flather MD, Yusuf S, Køber L, Pfeffer M, Hall A, Murray G, Torp-Pedersen C, Ball S, Pogue J, Moyé L, Braunwald E. Long-term ace-inhibitor therapy in patients with heart failure or left-ventricular dysfunction: A systematic overview of data from individual patients. *Lancet* 2000; **355**:1575-1581. DOI:10.1016/s0140-6736(00)02212-1.

6. McMurray JJ, Pfeffer MA. Heart failure. *Lancet* 2005; **365**:1877-1889. DOI:10.1016/S0140-6736(05)66621-4.

7. Wang T, Wu DQ, Jiang XJ, Zhang XZ, Li XY, Zhang JF, Zheng ZB, Zhuo R, Jiang H, Huang C. Novel thermosensitive hydrogel injection inhibits post-infarct ventricle remodelling. *European Journal of Heart Failure* 2009; **11**:14-19.

8. Dobner S, Bezuidenhout D, Govender P, Zilla P, Davies N. A synthetic non-degradable polyethylene glycol hydrogel retards adverse post-infarct left ventricular remodeling. *Journal of Cardiac Failure* 2009; **15**:629-636.

9. Kadner K, Dobner S, Franz T, Bezuidenhout D, Sirry MS, Zilla P, Davies NH. The beneficial effects of deferred delivery on the efficiency of hydrogel therapy post myocardial infarction. *Biomaterials* 2012; **33**:2060-2066. DOI:10.1016/j.biomaterials.2011.11.031.

10. Christman KL, Lee RJ. Biomaterials for the treatment of myocardial infarction. *Journal of the American College of Cardiology* 2006; **48**:907-913. DOI:10.1016/j.jacc.2006.06.005.

11. Nelson DM, Ma Z, Fujimoto KL, Hashizume R, Wagner WR. Intra-myocardial biomaterial injection therapy in the treatment of heart failure: Materials, outcomes and challenges. *Acta Biomaterialia* 2011; **7**:1-15. DOI:10.1016/j.actbio.2010.06.039.

12. Menasché P. Skeletal myoblasts as a therapeutic agent. *Progress in Cardiovascular Diseases* 2007; **50**:7-17.

13. Segers VF, Lee RT. Stem-cell therapy for cardiac disease. *Nature* 2008; **451**:937-942.

14. Wall ST, Walker JC, Healy KE, Ratcliffe MB, Guccione JM. Theoretical impact of the injection of material into the myocardium - a finite element model simulation. *Circulation* 2006; **114**:2627-2635.

15. Wenk JF, Eslami P, Zhang Z, Xu C, Kuhl E, Gorman Iii JH, Robb JD, Ratcliffe MB, Gorman RC, Guccione JM. A novel method for quantifying the in-vivo mechanical effect of material injected into a myocardial infarction. *Annals of Thoracic Surgery* 2011; **92**:935-941. DOI:10.1016/j.athoracsur.2011.04.089.

16. Kortsmit J, Davies NH, Miller R, Macadangdang JR, Zilla P, Franz T. The effect of hydrogel injection on cardiac function and myocardial mechanics in a computational post-infarction model. *Computer Methods in Biomechanics and Biomedical Engineering* 2013; **16**:1185-1195. DOI:10.1080/10255842.2012.656611.

17. Miller R, Davies NH, Kortsmit J, Zilla P, Franz T. Outcomes of myocardial infarction hydrogel injection therapy in the human left ventricle dependent on injectate distribution. *International Journal for Numerical Methods in Biomedical Engineering* 2013; **29**:870-884. DOI:10.1002/cnm.2551.

18. Saleh MG, Sharp S-K, Alhamud A, Spottiswoode BS, van der Kouwe AJW, Davies NH, Franz T, Meintjes EM. Long-term left ventricular remodelling in rat model of nonreperfused myocardial infarction: Sequential mr imaging using a 3t clinical scanner. *Journal of Biomedicine & Biotechnology* 2012; **2012**:10. DOI:10.1155/2012/504037.

19. Heiberg E, Sjogren J, Ugander M, Carlsson M, Engblom H, Arheden H. Design and validation of segment - freely available software for cardiovascular image analysis. *BMC Medical Imaging* 2010; **10**:1-13.

20. Omens JH, MacKenna DA, McCulloch AD. Measurement of strain and analysis of stress in resting rat left ventricular myocardium. *Journal of Biomechanics* 1993; **26**:665-676. DOI:10.1016/0021-9290(93)90030-i.

21. Chen J, Song S-K, Liu W, McLean M, Allen JS, Tan J, Wickline SA, Yu X. Remodeling of cardiac fiber structure after infarction in rats quantified with diffusion tensor mri. *American Journal of Physiology - Heart and Circulatory Physiology* 2003; **285**:H946-H954. DOI:10.1152/ajpheart.00889.2002.

22. Guccione JM, Costa KD, McCulloch AD. Finite element stress analysis of left ventricular mechanics in the beating dog heart. *Journal of Biomechanics* 1995; **28**:1167-1177.

23. Guccione J, Moonly S, Moustakidis P, Costa K, Moulton M, Ratcliffe M, Pasque M. Mechanism underlying mechanical dysfunction in the border zone of left ventricular aneurysm: A finite element model study. *Annals of Thoracic Surgery* 2001; **71**:654-662.

24. Usyk T, Mazhari R, McCulloch A. Effect of laminar orthotropic myofiber architecture on regional stress and strain in the canine left ventricle. *Journal of Elasticity* 2000; **61**:143-164.

25. Doll S, Schweizerhof K. On the development of volumetric strain energy functions. *Journal of Applied Mechanics* 2000; **67**:17-21.

26. Guccione JM, McCulloch AD. Mechanics of active contraction in cardiac muscle: Part i--constitutive relations for fiber stress that describe deactivation. *Journal of Biomechanical Engineering* 1993; **115**:72-81.

27. Ter Keurs HEDJ. *Calcium and contractility*, in *Cardiac metabolism*, Ter Keurs, H E D J, Editor. 1983, Wiley: New York. p. 73-99.

28. Ter Keurs HEDJ, Rijnsburger WH, Van Heuningen R, Nagelsmit MJ. *Tension development and sarcomere length in rat cardiac trabeculae: Evidence of length-dependent activation*, in *Cardiac dynamics*, Baan, J, Arntzenius, A C, Yellin, E L, Editors. 1980, Springer: The Hague. p. 25-36.

29. Cox MAJ, Driessen NJB, Bouten CVC, Baaijens FPT, *Mechanical characterization of anisotropic planar biological soft tissues using large indentation: An experimental validation study*, in *Proceedings of ICCB*, H. Rodrigues, M C, M. Doblare, J. Ambrosio, and M. Viceconti, Editor. 2005: Lisbon, Portugal. p. 339-350.

30. Ifkovits JL, Tous E, Minakawa M, Morita M, Robb JD, Koomalsingh KJ, Gorman JH, Gorman RC, Burdick JA. Injectable hydrogel properties influence infarct expansion and extent of postinfarction left ventricular remodeling in an ovine model. *Proceedings of the National Academy of Sciences of the United States of America* 2010; **107**:11507-11512. DOI:10.1073/pnas.1004097107.

31. Nash MP, Hunter PJ. Computational mechanics of the heart. *Journal of elasticity and the physical science of solids* 2000; **61**:113-141. DOI:10.1023/A:1011084330767.

32. Sirry MS, Davies NH, Kadner K, Dubuis L, Saleh MG, Meintjes EM, Spottiswoode BS, Zilla P, Franz T. Micro-structurally detailed model of a therapeutic hydrogel injectate in a rat biventricular cardiac geometry for computational simulations. *Computer Methods in Biomechanics and Biomedical Engineering* 2015; **18**:325-331. DOI:10.1080/10255842.2013.793765.

33. Wenk JF, Wall ST, Peterson RC, Helgerson SL, Sabbah HN, Burger M, Stander N, Ratcliffe MB, Guccione JM. A method for automatically optimizing medical devices for treating heart failure: Designing polymeric injection patterns. *Journal of Biomechanical Engineering* 2009; **131**:1210111-1210117.

34. Lee LC, Wall ST, Genet M, Hinson A, Guccione JM. Bioinjection treatment: Effects of post-injection residual stress on left ventricular wall stress. *Journal of Biomechanics* 2014; **47**:3115-3119. DOI:10.1016/j.jbiomech.2014.06.026.

**Table 1.** Left ventricle functional parameters predicted by different models: the healthy heart (H), 10% infarct without injectate (I10) and with 25%, 50% and 75% injectate (I10-G25, I10-G50, I10-G75), 20% infarct without injectate (I20) and with 50% injectate (I20-G50) and 38% infarct without injectate (I38) and with 25% injectate (I38-G28).

| **Model** | $E_{max}$ **(kPa/µl)** | $V_0$ **(µl)** | **SV (µl)** | **EF (%)** |
|---|---|---|---|---|
| H | 0.210 | 48.44 | 114.57 | 49.7 |
| I10 | 0.203 | 57.18 | 103.63 | 44.9 |
| I10-G25 | 0.205 | 50.45 | 102.83 | 46.4 |
| I10-G50 | 0.214 | 47.25 | 101.49 | 47.4 |
| I10-G75 | 0.217 | 48.35 | 101.41 | 47.3 |
| I20 | 0.202 | 67.60 | 67.34 | 29.2 |
| I20-G50 | 0.199 | 57.42 | 87.46 | 40.6 |
| I38 | 0.157 | 81.43 | 59.60 | 25.8 |
| I38-G25 | 0.145 | 72.40 | 61.71 | 26.7 |

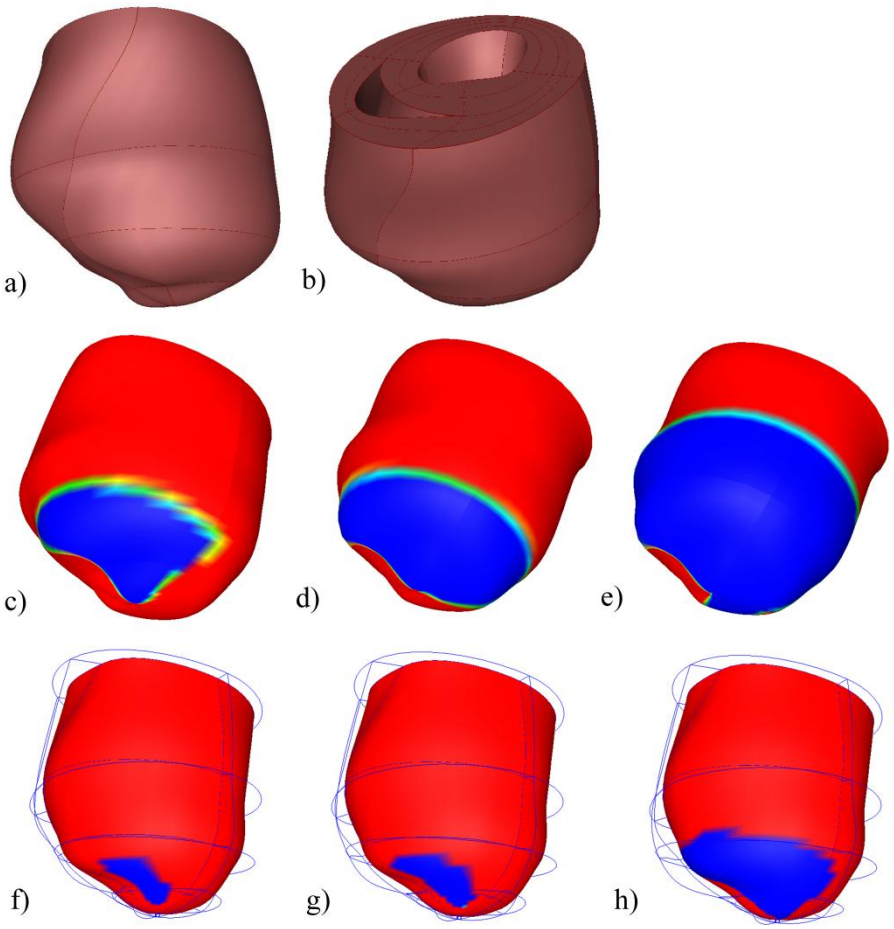


**Fig. 1.** Biventricular model of the rat heart: (a) side view showing the apex and (b) view on the base of the heart with the cavities of the left and right ventricles. Antero-apical view of the infarct area with infarct sizes of 10% (c), 20% (d) and 38% (e) (Red: healthy tissue. Dark blue: infarct area. Light blue, green and yellow: functional border zone). View of the hydrogel-treated region in the 10% infarct for injectate sizes of 25% (f), 50% (g) and 75% (h) (Displayed on the mid-wall surface. Red: myocardium. Dark blue: injectate treated region).

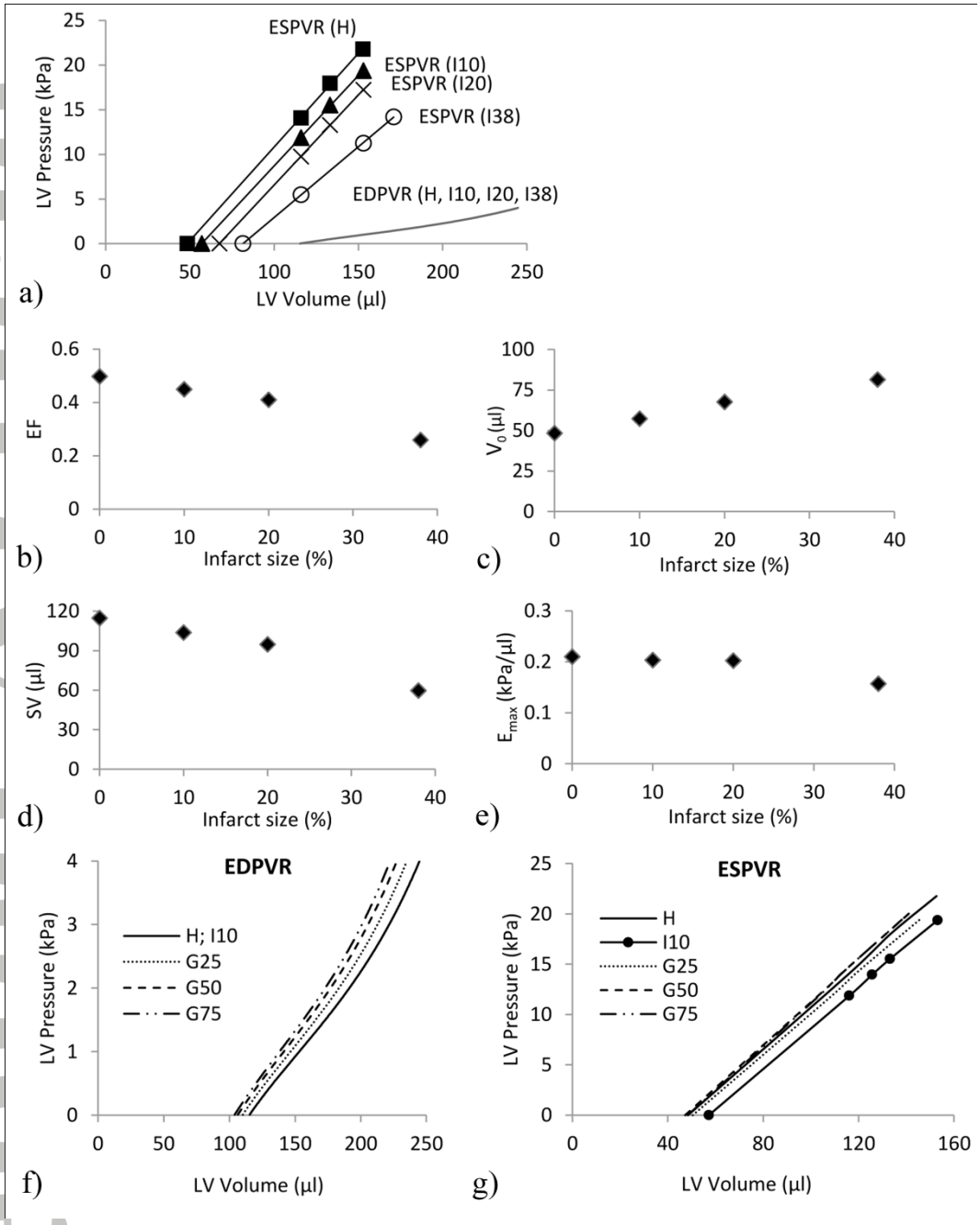


**Fig. 2.** Left ventricle functional parameters predicted by models of 10%, 20% and 38% untreated infarcts (a-e) and 10% infarct treated with 25%, 50% and 75% hydrogel injectate volumes (f, g): (a) End-systolic and end-diastolic pressure volume curves. The end-diastolic pressure volume curves are identical for all cases. (b) Ejection fraction. (c) Dead volume. (d) Stroke volume. (e) End-systolic elastance. (Note: Data for infarct size of 0% represent the healthy case.). (f) End-diastolic pressure volume relationship. The end-diastolic pressure volume curves for healthy case and untreated infarct are identical. (g) End-systolic pressure volume relationship. (H= healthy; I10, I20 and I38= untreated 10%, 20% and 38% infarct; G25, G50 and G75= 10% infarct treated with 25%, 50% and 75% injectate volume).

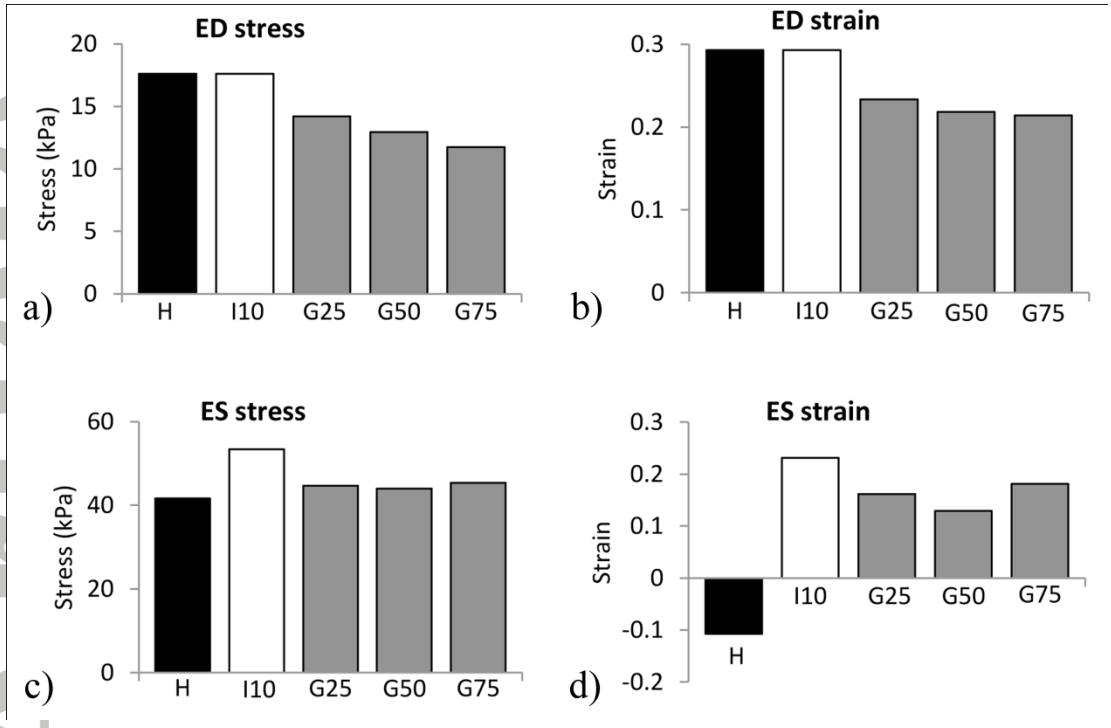


**Fig. 3.** End-diastolic (ED) and end-systolic (ES) maximum fibre stress and strain in the infarct region of the untreated and treated 10% infarct cases with 25%, 50% and 75% hydrogel injectates and in the corresponding region for the healthy case: (a) ED stress, (b) ED strain, (c) ES stress, (d) ES strain. (H= healthy; I10= untreated 10% infarct; G25, G50 and G75= 10% infarct with 25%, 50% and 75% injectate).

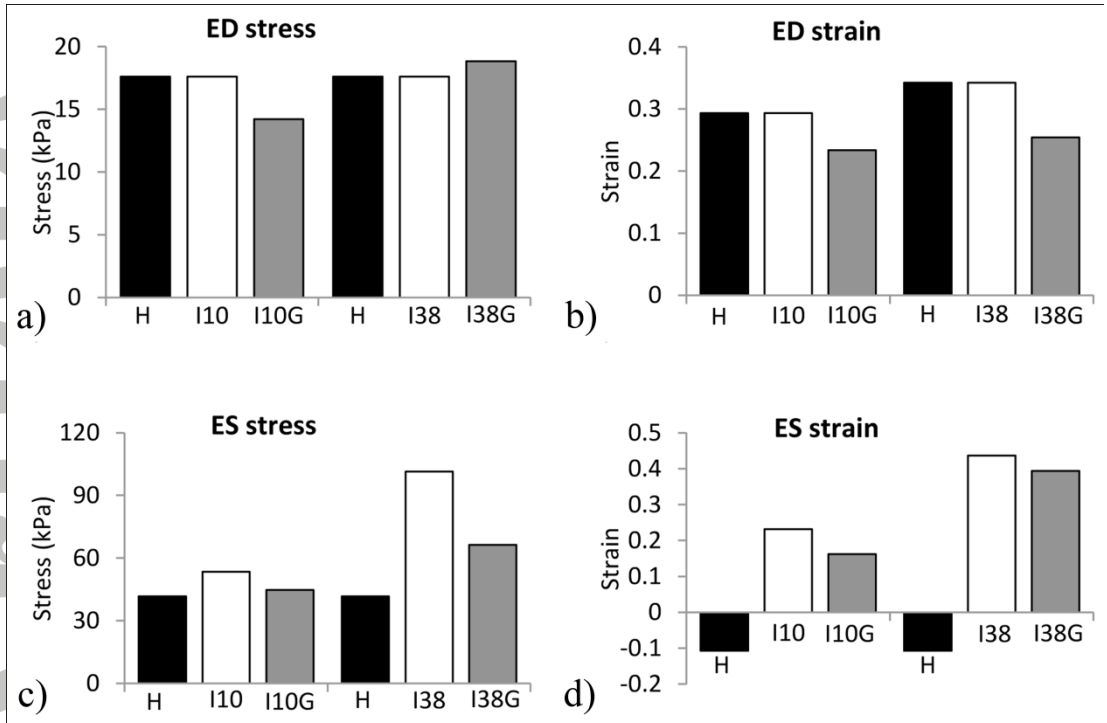


**Fig. 4.** End-diastolic (ED) and end-systolic (ES) maximum fibre stress and strain in the infarct region of the 10% and 38% untreated infarcts, the treated cases with 25% hydrogel injectate and in the corresponding region for the healthy case: (a) ED stress, (b) ED strain, (c) ES stress, (d) ES strain. (H= healthy; I10= untreated 10% infarct; I10G= 10% infarct treated with 25% injectate; I38= untreated 38% infarct; I38G= 38% infarct treated with 25% injectate).

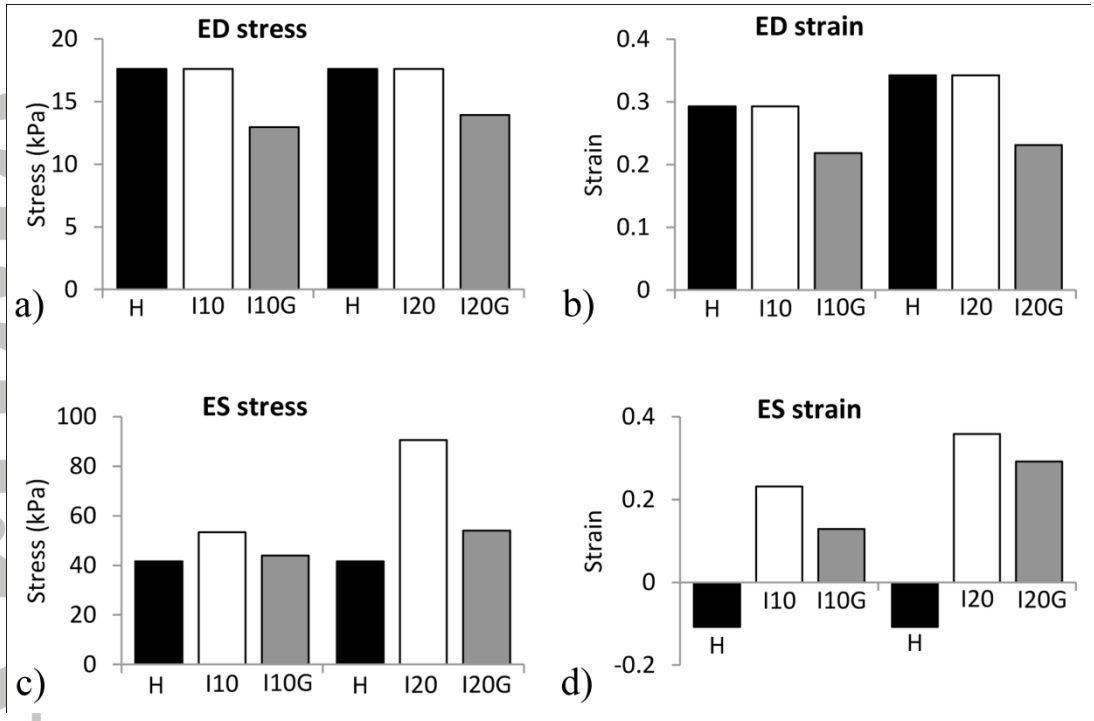


**Fig. 5.** End-diastolic (ED) and end-systolic (ES) maximum fibre stress and strain in the infarct region of the 10% and 20% untreated infarcts, the treated cases with 50% hydrogel injectate and in the corresponding region for the healthy case: (a) ED stress, (b) ED strain, (c) ES stress, (d) ES strain. (H= healthy; I10= untreated 10% infarct; I10G= 10% infarct treated with 50% injectate; I20= untreated 20% infarct; I20G= 20% infarct treated with 50% injectate).

# Excessive volume of hydrogel injectates may compromise the efficacy for the treatment of acute myocardial infarction

Peter Wise[1], Neil H. Davies[1], Mazin S. Sirry[2,3], Jeroen Kortsmit[1,#], Laura Dubuis[1,2], Chen-Ket Chai[4], Frank PT Baaijens[4], Thomas Franz[2,5,6,*]

[#] Claude Leon Postdoctoral Fellow

*Send correspondence to:
Thomas Franz, PhD
Tel: +27 21 650 1795
E-mail: thomas.franz@uct.ac.za

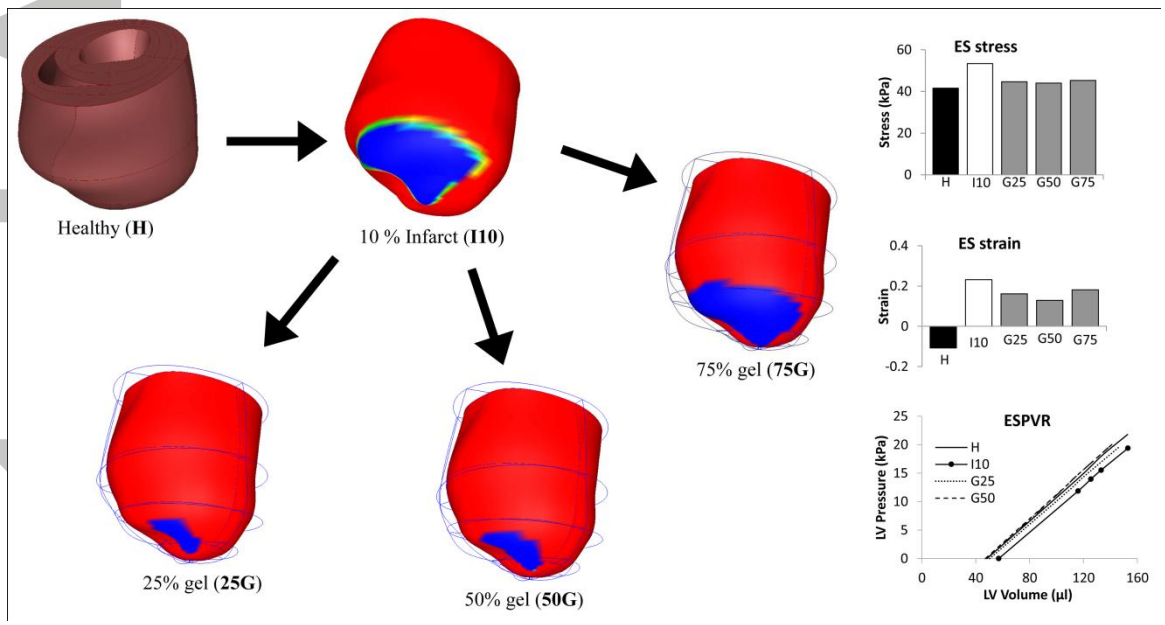


## GRAPHICAL ABSTRACT

The results of this study indicate that a threshold may exist for the volume of biomaterial injectates for treatment of acute myocardial infarction. For volumes exceeding that threshold, the therapeutic efficacy of the treatment does not further increase but may even decrease - both in terms of ventricular function and wall mechanics. In addition, the efficacy of biomaterial injectates in terms of reducing wall stress in the infarct was shown to increase with infarct size.